

# MMT observations of new extremely metal-poor emission-line galaxies in the Sloan Digital Sky Survey

Yuri I. Izotov

*Main Astronomical Observatory, National Academy of Sciences of Ukraine, 03680, Kyiv, Ukraine*

izotov@mao.kiev.ua

Trinh X. Thuan

*Astronomy Department, University of Virginia, Charlottesville, VA 22903*

txt@virginia.edu

## ABSTRACT

We present 6.5-meter MMT spectrophotometry<sup>1</sup> of 20 H II regions in 13 extremely metal-poor emission-line galaxies selected from the Data Release 5 of the Sloan Digital Sky Survey to have  $[\text{O III}]\lambda 4959/\text{H}\beta \lesssim 1$  and  $[\text{N II}]\lambda 6583/\text{H}\beta \lesssim 0.05$ . The electron temperature-sensitive emission line  $[\text{O III}]\lambda 4363$  is detected in 13 H II regions allowing a direct abundance determination. The oxygen abundance in the remaining H II regions is derived using a semi-empirical method. The oxygen abundance of the galaxies in our sample ranges from  $12 + \log \text{O}/\text{H} \sim 7.1$  to  $\sim 7.8$ , with 10 H II regions having an oxygen abundance lower than 7.5. The lowest oxygen abundances,  $12 + \log \text{O}/\text{H} = 7.14 \pm 0.03$  and  $7.13 \pm 0.07$ , are found in two H II regions of the blue compact dwarf galaxy SDSSJ0956+2849  $\equiv$  DDO 68, making it the second most-metal deficient emission-line galaxy known, after SBS 0335–052W.

*Subject headings:* galaxies: abundances — galaxies: irregular — galaxies: evolution — galaxies: formation — galaxies: ISM — H II regions — ISM: abundances

## 1. Introduction

Extremely metal-deficient emission-line galaxies at low redshifts are the most promising young galaxy candidates in the local Universe (Guseva et al. 2003; Izotov & Thuan 2004b). They are important to identify because of several reasons. First, studies of their nearly pristine interstellar medium (ISM) can shed light on the properties of the primordial ISM at the time of galaxy formation. It appears now that even the most metal-deficient galaxies in the local Universe formed

---

<sup>1</sup>The MMT is operated by the MMT Observatory (MMTO), a joint venture of the Smithsonian Institution and the University of Arizona.

from matter which was already pre-enriched by a previous star formation episode, e.g. by Population III stars (Thuan et al. 2005). It is thus quite important to establish firmly the level of this pre-enrichment by searching for the most metal-deficient emission-line galaxies. Second, because they have not undergone much chemical evolution, these galaxies are also the best objects for the determination of the primordial He abundance and for constraining cosmological models (e.g. Izotov & Thuan 2004a; Izotov et al. 2007). Third, in the hierarchical picture of galaxy formation, large galaxies form from the assembly of small dwarf galaxies. While much progress has been made in finding large populations of galaxies at high redshifts ( $z \gtrsim 3$ , Steidel et al. 2003), truly young galaxies in the process of forming remain elusive in the distant universe. The spectra of those far-away galaxies generally indicate the presence of a substantial amount of heavy elements, indicating previous star formation and metal enrichment. Therefore, extremely metal-deficient dwarf galaxies are possibly the closest examples we can find of the elementary primordial units from which galaxies formed. Their relative proximity allows studies of their stellar, gas and dust content with a sensitivity, spectral and spatial resolution that faint distant high-redshift galaxies do not permit.

Extremely metal-deficient emission-line galaxies are however very rare. Many surveys have been carried out to search for such galaxies without significant success. For more than three decades, one of the first blue compact dwarf (BCD) galaxies discovered, I Zw 18 (Sargent & Searle 1970) continued to hold the record as the most metal-deficient emission-line galaxy known, with an oxygen abundance  $12 + \log \text{O}/\text{H} = 7.17 \pm 0.01$  in its northwestern component and  $7.22 \pm 0.02$  in its southeastern component (Thuan & Izotov 2005). Only very recently, has I Zw 18 been displaced by the BCD SBS 0335–052W. This galaxy, with an oxygen abundance  $12 + \log \text{O}/\text{H} = 7.12 \pm 0.03$ , is now the emission-line galaxy with the lowest metallicity known (Izotov et al. 2005).

Because of the scarcity of extremely low-metallicity galaxies such as I Zw 18 and SBS 0335–052W, we stand a better chance of finding them in very large spectroscopic surveys. One of the best surveys suitable for such a search is the Sloan Digital Sky Survey (SDSS) (York et al. 2000). However, despite intensive studies of galaxies with a detected temperature-sensitive [O III]  $\lambda 4363$  emission line in their spectra, no emission-line galaxy with an oxygen abundance as low as that of I Zw 18 has been discovered in the SDSS Data Release 3 (DR3) and earlier releases. The lowest-metallicity emission-line galaxies found so far in these releases have oxygen abundances  $12 + \log \text{O}/\text{H} > 7.4$  (Kniazev et al. 2003, 2004; Izotov et al. 2004, 2006a). Only recently, Izotov et al. (2006b) have shown that two galaxies, J2104–0035 and J0113+0052, selected from the SDSS Data Release 4 (DR4), are very metal-poor, with  $12 + \log \text{O}/\text{H} = 7.26 \pm 0.03$  and  $7.17 \pm 0.09$ , respectively.

In order to find new candidates for extremely metal-deficient emission-line galaxies, we have carried out a systematic search for such objects in the SDSS Data Release 5 (DR5) (Adelman-McCarthy et al. 2007). We have chosen them on the basis of the relative fluxes of selected emission lines, as in Izotov et al. (2006b). All known extremely metal-deficient emission-line galaxies are characterized by relatively weak (compared to  $\text{H}\beta$ ) [O II]  $\lambda 3727$ , [O III]  $\lambda 4959$ ,  $\lambda 5007$  and [N II]  $\lambda 6583$  emission lines (e.g. Izotov & Thuan 1998a,b; Izotov et al. 2005; Pustilnik et al. 2005; Izotov et al. 2006b). These spectral properties select out uniquely low-metallicity dwarfs since no other type of

galaxy possesses them. In contrast to previous studies (Kniazev et al. 2003, 2004; Izotov et al. 2004, 2006a) which focus exclusively on objects with a detected [O III]  $\lambda 4363$  emission line, we have also considered objects which satisfy the criteria described above, but with spectra where [O III]  $\lambda 4363$  is weak or not detected. Since the [O II]  $\lambda 3727$  line is out of the observed wavelength range in SDSS spectra of galaxies with a redshift  $z$  lower than 0.02, we use two criteria, [O III]  $\lambda 4959/H\beta \lesssim 1$  and [N II]  $\lambda 6583/H\beta \lesssim 0.05$ , to pick out  $\sim 100$  galaxies from the DR5. The efficiency of this technique to pick out extremely low-metallicity galaxy candidates has been demonstrated by Izotov et al. (2006b).

While the SDSS spectra allow us to select very low metallicity galaxies, we need additional spectral observations for the following reasons: 1) a spectrum that goes further into the blue wavelength range is required to detect the [O II]  $\lambda 3727$  line. For a precise oxygen abundance determination, this line is needed to provide information on the singly ionized ionic population of oxygen. In principle, the [O II]  $\lambda 7320, 7330$  emission lines can be used instead. However, these lines are very weak or not detected in the SDSS spectra of low-metallicity candidates. 2) A better signal-to-noise ratio spectrum may allow the detection of a weak [O III]  $\lambda 4363$  emission line, which would permit a direct determination of the electron temperature. 3) Very often, low-metallicity candidates possess two or more H II regions with different degrees of excitation. However, SDSS spectra are usually obtained for only one H II region, chosen sometimes not in the most optimal way. A case in point is that of the galaxy J2104–0035. It has two H II regions. Only the spectrum of the lower excitation one, with no [O III]  $\lambda 4363$  emission, is available in the SDSS data base. Izotov et al. (2006b) obtained a ESO 3.6 m spectrum of the second H II region which turned out to have a higher excitation and a clearly detected [O III]  $\lambda 4363$  emission line, allowing a reliable abundance determination. This new observation of J2104–0035 has shown the galaxy to be very metal-poor.

For these reasons, we have started an observational program using the MMT to obtain new spectroscopic observations of a subsample of SDSS metal-poor galaxy candidates. The observations and data reduction are discussed in §2. The element abundances are derived in §3. Our main findings are given in §4.

## 2. Observations and Data Reduction

We have obtained new high signal-to-noise ratio spectrophotometric observations of 20 H II regions in 13 emission-line galaxies with the 6.5-meter MMT on the nights of 2006 December 15 – 16. The galaxies are listed in Table 1 in order of increasing right ascension, along with some of their general properties such as coordinates, redshifts, identifications of their SDSS spectra, and other designations. The SDSS images of the observed galaxies are shown in Fig. 1. Labels of individual H II regions are shown when several of them have been observed within the same galaxy. We show in Fig. 2 (available only in the on-line version) the SDSS spectra used to select the galaxies from the DR5. It is seen from the figure that the [O II]  $\lambda 3727$  emission line is out of the observed spectral

range and that the [N II]  $\lambda 6584$  emission line is weak in all spectra.

Ten out of the thirteen galaxies listed in Table 1 have been chosen from the DR5 with the selection criteria described before. Their oxygen abundances are not known before this work. The 3 remaining galaxies satisfy also the selection criteria, except for J2238+1400 where  $[\text{O III}]\lambda 4959/\text{H}\beta \sim 1.6$ . However, their oxygen abundances have been determined before. Two galaxies have been included in our observing program because they are among the five most metal-deficient emission-line galaxies known, and we believe that more information can be obtained about them with supplementary observations. Izotov et al. (2006b) have obtained  $12+\log(\text{O}/\text{H}) = 7.17\pm 0.09$  for J0113+0052 $\equiv$ UGC 772, and Pustilnik et al. (2005) have measured  $12+\log(\text{O}/\text{H}) = 7.21\pm 0.07$  for J0946+5452 $\equiv$ DDO 68. We wish to improve the abundance determination in these two galaxies with higher signal-to-noise ratio observations. The third galaxy is J2238+1400 $\equiv$ HS 2236+1344 which has been studied spectroscopically by Ugryumov et al. (2003), Izotov & Thuan (2004a) and Guseva et al. (2007). Izotov & Thuan (2004a) have found in its spectrum a strong high-ionization [Fe V]  $\lambda 4227$  emission line, with an ionization potential of 4 Ryd. We have included this galaxy in our observing program to search for the high-ionization [Ne V]  $\lambda 3346, 3425$  line emission which has an ionization potential of  $\sim 7$  Ryd, and to check for the consistency of the abundance determinations for this object by different authors, using different telescopes.

With the exception of J0254+0035 and J2238+1400, all galaxies in Table 1 are at a distance  $\lesssim 30$  Mpc. Five of them are within a distance of 10 Mpc, which makes them ideal for a study of their resolved stellar populations with the *Hubble Space Telescope*.

All observations have been made with the Blue Channel of the MMT spectrograph. The log of the observations is given in Table 2. We used a  $1''.5\times 300''$  slit and a 800 grooves/mm grating in first order. The above instrumental set-up gave a spatial scale along the slit of  $0''.6 \text{ pixel}^{-1}$ , a scale perpendicular to the slit of  $0.75\text{\AA} \text{ pixel}^{-1}$ , a spectral range of 3200–5200 $\text{\AA}$  and a spectral resolution of  $\sim 3\text{\AA}$  (FWHM). The seeing was in the range  $1''\text{--}1''.5$ . Total exposure times varied between 30 and 45 minutes. Each exposure was broken up into 2–3 subexposures, not exceeding 15 minutes, to allow for removal of cosmic rays. Several objects were observed at low airmasses  $< 1.3$  or with the slit oriented along the parallactic angle. The latter observations are labeled (P) in Table 2. The effect of atmospheric refraction for these observations is small. However, it can be important in the spectra of galaxies observed at high airmasses  $> 1.3$ . Fortunately, strong hydrogen lines are observed in some spectra (i.e. those of J0204–1009, J0747+5111) and correction for interstellar extinction with the use of those lines will automatically take into account the effect of atmospheric refraction. This is because interstellar extinction correction is performed in such a way so that the intensities of all observed hydrogen lines after correction are as close as possible to their theoretical recombination values, for a given electron temperature. However, in some other spectra obtained at high airmasses (those of J0301–0052, J0812+4836, J0911+3135, J0940+2935 and J0946+5452), the hydrogen lines are weaker, making such correction less certain. Three Kitt Peak IRS spectroscopic standard stars, G191B2B, Feige 110 and BD +28 4211 have been observed for flux calibration. Spectra of He–Ne–Ar comparison arcs were obtained before and after each observation to calibrate

the wavelength scale.

The two-dimensional spectra were bias subtracted and flat-field corrected using IRAF<sup>2</sup>. We then use the IRAF software routines IDENTIFY, REIDENTIFY, FITCOORD, TRANSFORM to perform wavelength calibration and correct for distortion and tilt for each frame. One-dimensional spectra were then extracted from each frame using the APALL routine. Before extraction, distinct two-dimensional spectra of the same H II region were carefully aligned using the spatial locations of the brightest part in each spectrum, so that spectra were extracted at the same positions in all subexposures. For all objects, we extracted the brightest part of the BCD, corresponding to a different spatial size for each object. In all cases,  $6'' \times 1''.5$  extraction apertures were used. All extracted spectra from the same object were then co-added. We have summed the individual spectra from each subexposure after removal of the cosmic rays hits with the IRAF routine CRMEDIAN. The spectra obtained from each subexposure were also checked for cosmic rays hits at the location of strong emission lines, but none was found.

The sensitivity curve was obtained by fitting with a high-order polynomial the observed spectral energy distribution of the bright hot white dwarf standard stars G191B2B, Feige 110 and BD +28 4211. Because the spectra of these stars have only a small number of a relatively weak absorption features, their spectral energy distributions are known with a very good accuracy (Oke 1990). Moreover, the response function of the CCD detector is smooth, so we could derive a sensitivity curve with a precision better than 1% over the whole optical range.

The spectra for the 20 H II regions observed with the MMT are shown in Figure 3. These spectra have been reduced to zero redshift and corrected for extinction.

The observed line fluxes  $F(\lambda)$ , normalized to  $F(H\beta)$  and multiplied by a factor of 100, and their errors, for the 20 H II regions shown in Fig. 3 are given in Table 3, available only in the electronic version on line. They were measured using the IRAF SPLOT routine. The line flux errors listed include statistical errors derived with SPLOT from non-flux calibrated spectra, in addition to errors introduced in the standard star absolute flux calibration, which we set to 1% of the line fluxes. These errors will be later propagated into the calculation of abundance errors. The line fluxes were corrected for both reddening (using the extinction curve of Whitford (1958)) and underlying hydrogen stellar absorption derived simultaneously by an iterative procedure as described in Izotov et al. (1994). The extinction coefficient is defined as  $C(H\beta) = 1.47E(B - V)$ , where  $E(B - V) = A(V)/3.2$  and  $A(V)$  is the extinction in the  $V$  band (Aller 1984). The corrected line fluxes  $100 \times I(\lambda)/I(H\beta)$ , equivalent widths  $EW(\lambda)$ , extinction coefficients  $C(H\beta)$ , and equivalent widths  $EW(\text{abs})$  of the hydrogen absorption stellar lines are also given in Table 3, along with the uncorrected  $H\beta$  fluxes.

---

<sup>2</sup>IRAF is distributed by National Optical Astronomical Observatory, which is operated by the Association of Universities for Research in Astronomy, Inc., under cooperative agreement with the National Science Foundation.

### 3. Physical Conditions and Element Abundances

To determine element abundances, we follow generally the procedures of Izotov et al. (1994, 1997) and Thuan et al. (1995). We adopt a two-zone photoionized H II region model: a high-ionization zone with temperature  $T_e(\text{O III})$ , where [O III] and [Ne III] lines originate, and a low-ionization zone with temperature  $T_e(\text{O II})$ , where [O II], [N II], [S II] and [Fe III] lines originate. In the H II regions with a detected [O III]  $\lambda 4363$  emission line, the temperature  $T_e(\text{O III})$  is calculated using the “direct” method based on the [O III]  $\lambda 4363/(\lambda 4959 + \lambda 5007)$  line ratio. In H II regions where the [O III]  $\lambda 4363$  emission line is not detected, we used an empirical relation obtained from the photoionized models of Stasińska & Izotov (2003) and based on the more readily observable [O II]  $\lambda 3727$  and [O III]  $\lambda\lambda 4959, 5007$  lines :

$$t_e(\text{O III}) = -1.36854 \log \left[ \frac{I(\lambda 3727) + I(\lambda 4959) + I(\lambda 5007)}{I(\text{H}\beta)} \right] + 2.62577, \quad (1)$$

where  $t_e(\text{O III}) = 10^{-4} T_e(\text{O III})$ . We adopt the error in the temperature determined by Eq. 1 to be equal to the dispersion of  $t_{es}$  of individual H II region models about the least-square fit. This dispersion is  $\sim 1000\text{K}$ . The error is then propagated into the calculation of abundance errors. We will refer hereafter to this method as the “semi-empirical method”, to emphasize the fact that only the electron temperature is derived empirically, while abundances are calculated in the same way as those of H II regions with a detected [O III]  $\lambda 4363$  emission line, and to distinguish it from the “empirical” methods where the oxygen abundance is derived directly from the strong oxygen line intensities (e.g., Pilyugin & Thuan 2005).

For  $T_e(\text{O II})$ , we use the relation between the electron temperatures  $T_e(\text{O III})$  and  $T_e(\text{O II})$  obtained by Izotov et al. (2006a) from the H II photoionization models of Stasińska & Izotov (2003). These are based on more recent stellar atmosphere models and improved atomic data as compared to the Stasińska (1990) models. As the [S II]  $\lambda 6717$  and  $\lambda 6731$  emission lines are not in the observed wavelength region of the MMT spectra,  $N_e(\text{S II})$  was set to  $10 \text{ cm}^{-3}$  for all H II regions. This is justified as element abundances do not depend on  $N_e$  as long as its value is lower than  $\sim 10^4 - 10^5 \text{ cm}^{-3}$ , which is the case for the vast majority of of the H II regions in the emission-line galaxies considered here (e.g. Izotov et al. 2006a). Ionic and total heavy element abundances are derived using expressions for ionic abundances and ionization correction factors obtained by Izotov et al. (2006a). The element abundances are given in Table 4 (available only in the electronic version on line) along with the adopted electron temperatures for different ions.

Consider first the results obtained with the direct method for the 13 H II regions with a detected [O III]  $\lambda 4363$  emission line. The derived oxygen abundances for these H II regions are shown in the second column of Table 5. The galaxy J2238+1400, with two high-excitation H II regions, was observed to check for the presence of the high-ionization [Ne v]  $\lambda 3346, \lambda 3425$  emission lines in its spectra. No such lines were detected (Fig. 3t,u). Thus, despite the presence of the [Fe v]  $\lambda 4227$  emission line in the spectrum of its H II region No. 1 (Table 3), implying ionizing radiation with photon energies  $> 4 \text{ Ryd}$ , no ionizing radiation with photon energies above  $7 \text{ Ryd}$  is present

in this galaxy. This is in contrast to the situation in the three low-metallicity BCDs SBS 0335–052E, Tol 1214–277 and HS 0837+4717 known thus far to contain both [Fe v] and [Ne v] emission (Thuan & Izotov 2005). The oxygen abundances  $12 + \log \text{O}/\text{H} = 7.45$  and  $7.56$  derived respectively in regions J2238+1400 No.1 and J2238+1400 No.2 are in good agreement with the values  $7.49$  and  $7.58$  derived by Guseva et al. (2007) for the same H II regions. A very similar oxygen abundance of  $7.47$  was obtained for region No.1 by Ugryumov et al. (2003) and Izotov & Thuan (2004a). This shows that the abundances obtained for this galaxy by different authors, using different telescopes, are very consistent. Two other galaxies, J0113+0052 and J0956+2849, have been observed before. Izotov et al. (2006b) have obtained  $12 + \log \text{O}/\text{H} = 7.17 \pm 0.09$  for J0113+0052 No.1. With our higher signal-to-noise ratio spectrum, we derive  $12 + \log \text{O}/\text{H} = 7.24 \pm 0.05$ . Pustilnik et al. (2005) have obtained  $12 + \log \text{O}/\text{H} = 7.23 \pm 0.06$  and  $7.21 \pm 0.07$  for H II regions No.1 and No.2 in J0956+2849 (we follow Pustilnik et al. 2005, for the nomenclature of the H II regions). We derive  $12 + \log \text{O}/\text{H} = 7.14 \pm 0.03$  and  $7.13 \pm 0.07$  from our higher resolution and higher signal-to-noise ratio spectra of the same H II regions. The new measured abundances make J0956+2849 the second most metal-deficient emission-line galaxy known after SBS 0335–052W (Izotov et al. 2005). It is more metal-deficient than I Zw 18 NW ( $12 + \log \text{O}/\text{H} = 7.17 \pm 0.01$ ), I Zw 18 SE ( $12 + \log \text{O}/\text{H} = 7.22 \pm 0.01$ ) and SBS 0335–052E ( $12 + \log \text{O}/\text{H} = 7.31 \pm 0.01$ ) (Thuan & Izotov 2005). Other galaxies with a detected [O III]  $\lambda 4363$  have not been observed previously. They have higher oxygen abundances, in the range  $12 + \log \text{O}/\text{H} = 7.51 - 7.75$ .

While the determination of oxygen abundance in H II regions with a detected [O III]  $\lambda 4363$  via the direct method is straightforward, the determination of oxygen abundances in those H II regions with no detected [O III]  $\lambda 4363$  emission has to rely on semi-empirical or empirical methods based on the intensities of the strong [O II]  $\lambda 3727$  and [O III]  $\lambda 4959$ ,  $\lambda 5007$  nebular emission lines. In order to evaluate the accuracy of the abundances based on these semi-empirical or empirical methods, we have compared oxygen abundances derived with these alternative methods with those obtained by the direct method for the H II regions with detected [O III]  $\lambda 4363$  emission in our sample.

First, we compare the oxygen abundances derived with the direct method (column 2 in Table 5) with those obtained by the semi-empirical method described above (column 6 in Table 5). We find a general good agreement between the two methods. Exceptions are the two high excitation H II regions in J2238+1400. In these cases, the electron temperatures derived by the semi-empirical method (Eq. 1) are  $\sim 4000 - 5000\text{K}$  lower than those derived from the [O III]  $\lambda 4363/(\lambda 4959 + \lambda 5007)$  ratio, yielding significantly higher oxygen abundances. These discrepancies may indicate that these two H II regions have anomalous properties. This may be the case if [O III]  $\lambda 4363$  emission is enhanced by some mechanism that is different from stellar radiation heating such as shock heating, or if the [O III]  $\lambda 4363/(\lambda 4959 + \lambda 5007)$  ratio is artificially enhanced by a reduction of the fluxes of the [O III]  $\lambda 4959$  and  $\lambda 5007$  emission lines by collisional de-excitation in a dense interstellar medium ( $N_e \gtrsim 10^5 \text{ cm}^{-3}$ ), as discussed by Thuan et al. (1996) in the case of the BCD Mrk 996. In these conditions, the oxygen abundance derived by the direct method will be lower than the true value. Another possible mechanism for the enhancement of [O III]  $\lambda 4363$  emission is nonthermal radiation

from a hidden active galactic nucleus (AGN). However, we do not favor this mechanism because the optical spectra of both H II regions in J2238+1400 do not show the usual features that are characteristic of an AGN Seyfert 2 optical spectrum: the [Ne v]  $\lambda 3346, 3425$  emission lines are not detected (see the inset in Fig. 3t), the He II  $\lambda 4686$  emission line is weak (its intensity is only  $\sim 1\%$  of that of H $\beta$ , Table 3), and other lines, such as [O I]  $\lambda 6300$ , [N II]  $\lambda 6584$  and [S II]  $\lambda 6717, 6731$  are many times weaker than those in a typical Seyfert 2 galaxy (see Fig. 2m). We note however that Spitzer observations of several BCDs (Hunt et al. 2006; Thuan et al. 2007) have shown that the [O IV]  $\lambda 25.9 \mu\text{m}$  emission line, with an ionization potential of  $\sim 4$  Ryd is present in the MIR spectrum, while the [Fe IV]  $\lambda 4227$  and He II  $\lambda 4686$  emission lines with about the same ionization potential are conspicuously absent from the optical spectrum. This suggests that, in those BCDs, there may be a dust-enshrouded AGN that is optically invisible and which may be responsible for the hard radiation giving rise to the MIR line. If we exclude the two H II regions in J2238+1400, the average difference between the semi-empirical abundances and those derived by the direct method is 0.06 dex. The semi-empirical method also gives consistent oxygen abundances for multiple H II regions within the same galaxy, including those where the [O III]  $\lambda 4363$  emission line is not detected (see the galaxies J0113+0052 and in J0956+2849).

Next, we compare the abundances determined by the direct method with those derived using empirical methods. Recently, several groups have proposed empirical relations for the determination of  $12 + \log \text{O}/\text{H}$  using the nebular [O II]  $\lambda 3727$  and [O III]  $\lambda 4959, \lambda 5007$  emission line intensities:

$$12 + \log \frac{\text{O}}{\text{H}} = \frac{R_3 + 106.4P + 106.8P^2 - 3.40P^3}{17.72P + 6.60P^2 + 6.95P^3 - 0.302R_3}, \quad (2)$$

(Pilyugin & Thuan 2005),

$$\log R_{23} = 1.2299 - 4.1926y + 1.0246y^2 - 0.063169y^3, \quad (3)$$

(Nagao et al. 2006), and

$$12 + \log \frac{\text{O}}{\text{H}} = 6.486 + 1.401 \log R_{23}, \quad (4)$$

(Yin et al. 2007).

In Eqs. 2 – 4,  $R_3 = [I(\lambda 4959) + I(\lambda 5007)]/I(\text{H}\beta)$ ,  $R_{32} = R_3 + I(\lambda 3727)/I(\text{H}\beta)$ ,  $P = R_3/R_{32}$ ,  $y=12+\log \text{O}/\text{H}$ . We have derived oxygen abundances for all H II regions in our sample using the above equations. The results are shown in columns 3 – 5 of Table 5. Comparison with the abundances derived by the direct method shows that the empirical method of Pilyugin & Thuan (2005) does not work well in some cases. In particular, while the direct method gives abundances that are consistent and in a narrow range for the multiple H II regions in J0747+5111 and J0956+2849, the spread of the abundances for the same H II regions derived with the Pilyugin-Thuan relation is much larger (column 3 of Table 5). The latter relation also gives a larger spread of oxygen abundances for the multiple H II regions in J0113+0052, as compared to those obtained with the semi-empirical method. The average difference between the empirical abundances derived with the Pilyugin-Thuan relation and those derived by the direct method is 0.10 dex, excluding the two H II



regions in J2238+1400. Clearly, the empirical relation derived by Pilyugin & Thuan (2005) is not as accurate as the semi-empirical method in the extremely low metallicity regime considered here. This is because the galaxy sample used by Pilyugin & Thuan (2005) to calibrate their relation contained very few galaxies with  $12 + \log \text{O}/\text{H} \lesssim 7.5$ . The empirical relation derived by Nagao et al. (2006) gives consistent abundances in different H II regions of the same galaxy (column 4 of Table 5). However, these abundances are systematically lower than those derived by the direct method. The average difference between the empirical abundances derived using the Nagao et al. (2006) relation and those derived by the direct method is 0.13 dex, excluding the two H II regions in J2238+1400. The empirical relation derived by Yin et al. (2007) appears to give abundances that are most consistent with those derived by the direct method (column 5 of Table 5). The average difference between the empirical abundances derived with the relation by Yin et al. (2007) and those derived by the direct method is 0.07 dex, only slightly higher than that between the direct and semi-empirical methods.

Thus, we conclude that for our low-metallicity objects, the semi-empirical method is more appropriate for oxygen abundance determination because it gives more consistent abundances as compared to empirical methods. Therefore, for the H II regions with non-detected  $[\text{O III}] \lambda 4363$  emission, we adopt the oxygen abundances derived with the semi-empirical method, and for the remaining H II regions those derived with the direct method. However, it should be kept in mind that the oxygen abundances derived with the direct method for the two H II regions of J2238+1400 may be underestimated.

Examination of Table 5 shows that our sample contains at least 10 H II regions with oxygen abundance less than 7.5. However, no H II region with an oxygen abundance  $12 + \log \text{O}/\text{H} < 7.1$  has been found. This supports the idea discussed by, e.g., Thuan et al. (2005) that the matter from which dwarf emission-line galaxies formed was pre-enriched to the level  $12 + \log \text{O}/\text{H} \gtrsim 7.0$  (or  $\sim 2\%$  of the abundance  $12 + \log \text{O}/\text{H} = 8.65$  of the Sun, Asplund et al. 2005). Based on FUSE spectroscopic data, Thuan et al. (2005) showed that BCDs spanning a wide range in ionized gas metallicities all have H I envelopes with about the same neutral gas metallicity of  $\sim 7.0$ . This is also the metallicity found in Ly $\alpha$  absorbers. Taken together, the available data suggest that there may have been previous enrichment of the primordial neutral gas to a common metallicity level, possibly by Population III stars.

#### 4. Conclusions

We present spectroscopic observations with the 6.5m MMT of a sample of 20 H II regions in 13 dwarf emission-line galaxies. These galaxies were selected from the Data Release 5 (DR5) of the Sloan Digital Sky Survey (SDSS) using the two criteria  $[\text{O III}] \lambda 4959/\text{H}\beta \lesssim 1$  and  $[\text{N II}] \lambda 6583/\text{H}\beta \lesssim 0.05$ . These spectral properties select out extremely low-metallicity galaxies, with oxygen abundances comparable to those of the most metal-deficient emission-line galaxies known, SBS 0335–052W and I Zw 18. The above criteria select out  $\sim 100$  galaxies from the DR5, of which the 13

objects discussed here form a subsample.

We find that 10 H II regions have oxygen abundances  $12 + \log O/H$  lower than 7.5. We confirm the very low oxygen abundance found previously in two galaxies, J0113+0052 $\equiv$ UGC 772 and J0956+2849 $\equiv$ DDO 68, by Izotov et al. (2006b) and Pustilnik et al. (2005) respectively. In particular, we find that the oxygen abundance in the brightest H II region of J0956+2849 is  $7.14 \pm 0.03$ , making this galaxy the second most-metal deficient emission-line galaxy known, after SBS 0335–052W, and ahead of I Zw 18 NW, I Zw 18 SE and SBS 0335–052 E. However, no H II region with an oxygen abundance  $12 + \log O/H < 7.1$  has been found. The existing data on extremely metal-deficient emission-line galaxies appears to suggest the existence of an oxygen abundance floor. This supports the idea that the matter from which dwarf emission-line galaxies formed was pre-enriched to a level  $12 + \log O/H \sim 7.0$  (e.g., Thuan et al. 2005).

The MMT time was available thanks to a grant from the Frank Levinson Fund of the Peninsula Community Foundation to the Astronomy Department of the University of Virginia. The research has been supported by NSF grant AST-02-05785. Y.I.I. thanks the hospitality of the Astronomy Department of the University of Virginia. Funding for the Sloan Digital Sky Survey (SDSS) and SDSS-II has been provided by the Alfred P. Sloan Foundation, the Participating Institutions, the National Science Foundation, the U.S. Department of Energy, the National Aeronautics and Space Administration, the Japanese Monbukagakusho, and the Max Planck Society, and the Higher Education Funding Council for England.

## REFERENCES

- Adelman-McCarthy, J. K., et al. 2007, ApJS, submitted
- Aller, L. H. 1984, Physics of Thermal Gaseous Nebulae (Dordrecht: Reidel)
- Asplund, M., Grevesse, N., & Sauval, A. J. 2005, ASP Conf. Ser. 336: Cosmic Abundances as Records of Stellar Evolution and Nucleosynthesis, 336, 25
- Guseva, N. G., Papaderos, P., Izotov, Y. I., et al. 2003, A&A, 407, 105
- Guseva, N. G., Izotov, Y. I., Papaderos, P., & Fricke, K. J. 2007, A&A, 464, 885
- Hunt, L. K., Thuan, T. X., Sauvage, M., & Izotov, Y. I. 2006, ApJ, 653, 222
- Izotov, Y. I., & Thuan, T. X. 1998a, ApJ, 497, 227
- . 1998b, ApJ, 500, 188
- . 2004a, ApJ, 602, 200
- . 2004b, ApJ, 616, 768

- Izotov, Y. I., Thuan, T. X., & Lipovetsky, V. A. 1994, *ApJ*, 435, 647
- . 1997, *ApJS*, 108, 1
- Izotov, Y. I., Stasińska, G., Guseva, N. G., & Thuan, T. X. 2004, *A&A*, 632, 210
- Izotov, Y. I., Thuan, T. X., & Guseva, N. G. 2005, *ApJ*, 632, 210
- Izotov, Y. I., Stasińska, G., Meynet, G., Guseva, N. G., & Thuan, T. X. 2006a, *A&A*, 448, 955
- Izotov, Y. I., Papaderos, P., Guseva, N. G., Fricke, K. J., & Thuan, T. X. 2006b, *A&A*, 454, 137
- Izotov, Y. I., Thuan, T. X., & Stasińska, G. 2007, *ApJ*, in press; preprint astro-ph/0702072
- Kniazev, A. Y., Grebel, E. K., Hao, L., Strauss, M. A., Brinkmann, J., & Fukugita, M. 2003, *ApJ*, 593, 73
- Kniazev, A. Y., Pustilnik, S. A., Grebel, E. K., Lee, H., & Pramskij, A. G. 2004, *ApJS*, 153, 429
- Nagao, T., Maiolino, R., & Marconi, A. 2006, *A&A*, 459, 85
- Oke, J. B. 1990, *AJ*, 99, 1621
- Pilyugin, L. S., & Thuan, T. X. 2005, *ApJ*, 631, 231
- Pustilnik, S. A., Kniazev, A. Y., & Pramskij, A. G. 2005, *A&A*, 443, 91
- Sargent, W. L. W., & Searle, L. 1970, *ApJ*, 162, L155
- Stasińska G. 1990, *A&AS*, 83, 501
- Stasińska, G., & Izotov, Y. I. 2003, *A&A*, 397, 71
- Steidel, C. C., Adelberger, K. L., Shapley, A. E., et al. 2003, *ApJ*, 592, 728
- Thuan, T. X., Hunt, L. K. & Izotov, Y. I. 2007, in preparation
- Thuan, T. X., Izotov, Y. I. 2005, *ApJS*, 161, 240
- Thuan, T. X., Izotov, Y. I., & Lipovetsky, V. A. 1995, *ApJ*, 445, 108
- . 1996, *ApJ*, 463, 120
- Thuan, T. X., Lecavelier des Etangs, A., & Izotov, Y. I. 2005, *ApJ*, 621, 269
- Ugryumov, A. V., Endels, D., Pustilnik, S. A., Kniazev, A. Y., Pramskij, A. G., & Hagen, H.-J. 2003, *A&A*, 397, 463
- Whitford, A. E. 1958, *AJ*, 63, 201

Yin, S. Y., Liang, Y. C., Hammer, F., Brinchmann, J., Zhang, B., Deng, L. C., & Flores, H. 2007, A&A, 462, 535

York, D. G., et al. 2000, AJ, 120, 1579

Table 1. General Characteristics of Galaxies

SDSS Name	R.A. (J2000.0)	DEC. (J2000.0)	Redshift	SDSS Spectrum ID	Other Names
SDSSJ0113+0052	01 13 40.44	+00 52 39.2	0.0037630	53001-1499-525	UGC 772
SDSSJ0204–1009	02 04 25.61	–10 09 35.0	0.0063795	52149-0666-088	KUG 0201–103
SDSSJ0254+0035	02 54 28.94	+00 35 50.5	0.0148437	53035-1512-400	
SDSSJ0301–0052	03 01 49.01	–00 52 57.4	0.0072615	52616-1067-204	
SDSSJ0313+0010	03 13 01.60	+00 10 40.2	0.0077796	52203-0710-597	
SDSSJ0747+5111	07 47 33.18	+51 11 24.8	0.0014436	53327-1869-282	KUG 0743+513
SDSSJ0812+4836	08 12 39.53	+48 36 45.5	0.0017567	51885-0440-170	
SDSSJ0859+3923	08 59 46.93	+39 23 05.6	0.0019601	52669-1198-590	
SDSSJ0911+3135	09 11 59.42	+31 35 35.9	0.0025028	52976-1591-097	
SDSSJ0940+2935	09 40 12.84	+29 35 30.3	0.0018161	53415-1942-055	KUG 0937+298
SDSSJ0946+5452	09 46 22.87	+54 52 08.4	0.0054097	52282-0769-376	KUG 0942+551
SDSSJ0956+2849	09 56 46.05	+28 49 43.8	0.0016006	53431-1947-040	DDO 68
SDSSJ2238+1400	22 38 31.12	+14 00 29.8	0.0206160	53239-1893-476	HS 2236+1344

Table 2. Journal of Observations

SDSS Name	Date	Exposure	Airmass	P.A.
SDSSJ0113+0052	2006, 15 Dec	2460	1.17	+63.0
SDSSJ0204–1009	15 Dec	1800	1.40	–11.3
SDSSJ0254+0035	15 Dec	2700	1.18	–22.5 (P)
SDSSJ0301–0052	16 Dec	2700	1.41	+48.4
SDSSJ0313+0010	15 Dec	1800	1.18	+04.8 (P)
SDSSJ0747+5111	16 Dec	2700	1.78	–59.4
SDSSJ0812+4836	15 Dec	1800	1.38	+67.3
SDSSJ0859+3923	15 Dec	1800	1.44	–79.0 (P)
SDSSJ0911+3135	16 Dec	1800	1.42	+00.0
SDSSJ0940+2935	16 Dec	1800	1.39	+24.2
SDSSJ0946+5452	16 Dec	1800	1.71	+58.2
SDSSJ0956+2849	16 Dec	2700	1.29	–00.8
SDSSJ2238+1400	15 Dec	1800	1.17	+00.0

Table 3. Emission Line Intensities and Equivalent Widths

Ion	$F(\lambda)/F(H\beta)$	$I(\lambda)/I(H\beta)$	EW <sup>a</sup>	$F(\lambda)/F(H\beta)$	$I(\lambda)/I(H\beta)$	EW <sup>a</sup>
GALAXY						
	J0113+0052 No.1			J0113+0052 No.2		
3727 [O II]	50.41 ± 1.88	78.78 ± 3.02	54.1	203.01 ± 6.89	187.30 ± 7.26	72.1
3835 H9	6.83 ± 1.10	10.17 ± 1.96	8.1	...	...	...
3868 [Ne III]	12.60 ± 1.06	18.49 ± 1.58	11.2	...	...	...
3889 He I + H8	13.18 ± 0.91	19.19 ± 1.83	12.9	...	...	...
3968 [Ne III] + H7	13.89 ± 0.87	19.54 ± 1.67	14.7	...	...	...
4101 Hδ	20.73 ± 1.03	27.58 ± 1.83	19.4	19.57 ± 1.74	27.81 ± 3.30	7.3
4340 Hγ	38.70 ± 1.21	46.82 ± 1.88	33.8	41.30 ± 2.16	46.74 ± 3.04	17.4
4363 [O III]	5.75 ± 0.60	6.90 ± 0.73	4.3	...	...	...
4471 He I	3.36 ± 0.55	3.86 ± 0.64	2.7	...	...	...
4861 Hβ	100.00 ± 2.34	100.00 ± 2.57	83.4	100.00 ± 3.38	100.00 ± 3.88	47.1
4959 [O III]	73.86 ± 1.85	71.46 ± 1.81	60.5	46.75 ± 2.06	43.14 ± 2.06	17.1
5007 [O III]	212.88 ± 4.54	202.67 ± 4.37	194.6	132.55 ± 4.25	122.30 ± 4.25	49.4
$C(H\beta)$		0.630			0.000	
$F(H\beta)^b$		0.07			0.03	
EW(abs) Å		0.00			3.95	
GALAXY						
	J0113+0052 No.4			J0204-1009 No.1		
3727 [O II]	112.24 ± 4.56	107.64 ± 4.76	75.9	213.20 ± 11.39	164.95 ± 12.05	9.2
3868 [Ne III]	14.09 ± 1.92	13.51 ± 1.93	13.8	27.71 ± 5.19	21.44 ± 5.21	0.9
4340 Hγ	41.84 ± 2.00	47.36 ± 4.05	33.0	36.23 ± 3.63	55.14 ± 9.01	2.1
4861 Hβ	100.00 ± 3.59	100.00 ± 4.18	139.3	100.00 ± 5.49	100.00 ± 7.87	6.8
4959 [O III]	73.08 ± 2.94	70.09 ± 2.94	83.5	64.56 ± 4.45	49.95 ± 4.45	3.4
5007 [O III]	210.48 ± 6.37	201.86 ± 6.37	149.2	205.73 ± 9.53	159.17 ± 9.53	11.4
$C(H\beta)$		0.000			0.000	
$F(H\beta)^b$		0.03			0.03	
EW(abs) Å		5.95			2.00	
GALAXY						
	J0204-1009 No.2			J0254+0035		
3727 [O II]	139.72 ± 2.95	139.72 ± 3.09	63.3	166.40 ± 6.42	153.25 ± 6.91	20.6
3750 H12	2.01 ± 0.53	2.01 ± 0.81	1.0	...	...	...
3771 H11	3.15 ± 0.70	3.15 ± 0.93	1.6	...	...	...
3798 H10	4.72 ± 0.61	4.72 ± 0.86	2.4	...	...	...
3835 H9	6.32 ± 0.78	6.32 ± 1.00	3.1	...	...	...
3868 [Ne III]	23.40 ± 0.90	23.40 ± 0.91	9.3	10.44 ± 2.09	9.59 ± 2.14	1.0
3889 He I + H8	19.66 ± 0.85	19.66 ± 1.06	9.9	11.48 ± 1.74	23.95 ± 5.47	1.6
3968 [Ne III] + H7	22.84 ± 0.99	22.84 ± 1.17	11.7	5.32 ± 1.24	19.04 ± 8.45	0.7
4101 Hδ	28.84 ± 0.95	28.84 ± 1.08	18.1	15.05 ± 2.19	27.36 ± 5.35	2.0
4340 Hγ	46.82 ± 1.11	46.82 ± 1.23	28.0	38.05 ± 2.36	46.74 ± 3.65	5.7
4363 [O III]	6.53 ± 0.51	6.53 ± 0.52	3.5	...	...	...
4471 He I	3.70 ± 0.58	3.70 ± 0.58	2.0	...	...	...
4861 Hβ	100.00 ± 1.94	100.00 ± 1.97	83.4	100.00 ± 3.71	100.00 ± 4.30	17.7
4959 [O III]	94.11 ± 1.86	94.11 ± 1.86	76.5	45.99 ± 2.57	41.24 ± 2.57	6.5
5007 [O III]	272.63 ± 4.86	272.63 ± 4.86	222.6	143.69 ± 5.08	128.73 ± 5.07	21.5
5015 He I	1.97 ± 0.31	1.97 ± 0.31	1.6	...	...	...

Table 3—Continued

Ion	$F(\lambda)/F(H\beta)$	$I(\lambda)/I(H\beta)$	EW <sup>a</sup>	$F(\lambda)/F(H\beta)$	$I(\lambda)/I(H\beta)$	EW <sup>a</sup>
$C(H\beta)$		0.000			0.035	
$F(H\beta)^b$		0.20			0.03	
EW(abs) Å		0.00			2.00	
GALAXY						
	J0301-0052			J0313+0010		
3727 [O II]	45.17 ± 2.48	59.92 ± 3.55	37.3	243.68 ± 12.33	203.20 ± 13.13	19.8
3868 [Ne III]	23.35 ± 1.73	29.55 ± 2.34	17.8	...	...	...
3889 He I + H8	12.20 ± 1.62	21.42 ± 3.36	9.2	...	...	...
3968 [Ne III] + H7	15.39 ± 1.78	25.59 ± 3.52	10.2	...	...	...
4101 Hδ	20.49 ± 1.74	27.12 ± 2.54	28.9	...	...	...
4340 Hγ	37.00 ± 1.11	47.13 ± 2.07	22.1	35.04 ± 3.52	49.12 ± 7.56	2.9
4363 [O III]	8.63 ± 1.00	9.38 ± 1.15	5.1	...	...	...
4861 Hβ	100.00 ± 2.84	100.00 ± 3.22	65.7	100.00 ± 5.54	100.00 ± 7.51	10.0
4959 [O III]	132.88 ± 3.53	122.78 ± 3.47	82.1	64.61 ± 4.46	53.88 ± 4.46	5.1
5007 [O III]	395.54 ± 9.32	361.08 ± 9.06	230.6	186.08 ± 8.79	155.17 ± 8.80	14.2
$C(H\beta)$		0.475			0.000	
$F(H\beta)^b$		0.06			0.02	
EW(abs) Å		3.65			2.00	
GALAXY						
	J0747+5111 No.1			J0747+5111 No.2		
3727 [O II]	195.99 ± 3.92	240.79 ± 5.27	37.2	157.69 ± 2.89	160.82 ± 3.13	75.9
3771 H11	...	...	...	2.44 ± 0.54	4.99 ± 1.37	1.2
3798 H10	...	...	...	4.24 ± 0.56	6.74 ± 1.10	2.2
3835 H9	...	...	...	5.24 ± 0.48	7.70 ± 0.93	2.8
3868 [Ne III]	29.31 ± 1.38	34.79 ± 1.73	4.6	32.59 ± 0.93	33.09 ± 0.97	16.8
3889 He I + H8	14.77 ± 1.07	23.37 ± 2.12	3.1	17.65 ± 0.67	20.24 ± 0.95	9.6
3968 [Ne III] + H7	15.41 ± 1.17	24.06 ± 2.27	3.0	24.20 ± 0.76	26.80 ± 1.01	13.3
4101 Hδ	21.60 ± 1.07	29.86 ± 1.87	4.6	23.87 ± 0.67	26.06 ± 0.87	15.0
4340 Hγ	39.29 ± 1.11	47.11 ± 1.69	8.6	45.67 ± 0.93	47.31 ± 1.05	36.3
4363 [O III]	7.29 ± 0.76	7.74 ± 0.84	1.3	8.14 ± 0.43	8.14 ± 0.44	5.3
4471 He I	2.07 ± 0.50	2.15 ± 0.55	0.4	3.37 ± 0.36	3.36 ± 0.37	2.4
4686 He II	...	...	...	0.89 ± 0.22	0.89 ± 0.23	0.7
4861 Hβ	100.00 ± 1.93	100.00 ± 2.14	26.6	100.00 ± 1.73	100.00 ± 1.77	101.4
4959 [O III]	125.97 ± 2.35	119.01 ± 2.32	27.4	129.79 ± 2.19	127.91 ± 2.19	122.6
5007 [O III]	381.73 ± 6.63	357.49 ± 6.49	83.1	387.31 ± 6.24	381.25 ± 6.23	358.1
5015 He I	...	...	...	2.42 ± 0.23	2.38 ± 0.23	2.3
$C(H\beta)$		0.345			0.045	
$F(H\beta)^b$		0.28			0.29	
EW(abs) Å		1.05			1.25	
GALAXY						
	J0812+4836			J0859+3923		
3727 [O II]	161.92 ± 5.47	194.96 ± 7.50	31.6	307.16 ± 11.73	276.72 ± 12.51	41.5
3868 [Ne III]	5.64 ± 1.38	6.54 ± 1.75	0.8	18.41 ± 3.37	16.59 ± 3.37	1.7
3889 He I + H8	6.22 ± 2.35	20.45 ± 9.64	1.2	...	...	...
3968 [Ne III] + H7	8.79 ± 1.85	20.59 ± 5.50	2.0	...	...	...
4101 Hδ	14.15 ± 1.91	27.21 ± 4.82	2.8	17.10 ± 2.42	27.17 ± 5.25	2.2



Table 3—Continued

Ion	$F(\lambda)/F(H\beta)$	$I(\lambda)/I(H\beta)$	EW <sup>a</sup>	$F(\lambda)/F(H\beta)$	$I(\lambda)/I(H\beta)$	EW <sup>a</sup>
4340 H $\gamma$	$34.67 \pm 2.04$	$46.60 \pm 3.59$	7.2	$39.76 \pm 2.72$	$46.74 \pm 4.14$	5.4
4861 H $\beta$	$100.00 \pm 3.25$	$100.00 \pm 3.79$	25.8	$100.00 \pm 4.23$	$100.00 \pm 5.03$	15.0
4959 [O III]	$28.99 \pm 1.71$	$26.23 \pm 1.69$	6.2	$56.49 \pm 2.98$	$50.89 \pm 2.98$	6.9
5007 [O III]	$93.25 \pm 3.09$	$83.59 \pm 3.02$	19.8	$181.47 \pm 6.75$	$163.49 \pm 6.76$	22.5
$C(H\beta)$		0.375			0.000	
$F(H\beta)^b$		0.07			0.03	
EW(abs) Å		2.15			1.65	
GALAXY						
	J0911+3135			J0940+2935		
3727 [O II]	$219.22 \pm 7.75$	$279.68 \pm 10.95$	21.9	$165.62 \pm 3.23$	$185.55 \pm 3.93$	39.9
3835 H9	...	...	...	$2.99 \pm 0.68$	$8.49 \pm 2.46$	0.8
3868 [Ne III]	$10.11 \pm 3.28$	$12.39 \pm 4.23$	0.8	$14.33 \pm 0.90$	$15.73 \pm 1.03$	3.2
3889 He I + H8	$10.00 \pm 1.81$	$19.05 \pm 5.07$	1.1	$12.69 \pm 0.76$	$19.20 \pm 1.55$	3.4
3968 [Ne III] + H7	$6.38 \pm 1.16$	$13.99 \pm 4.52$	0.7	$13.64 \pm 0.77$	$19.98 \pm 1.52$	3.7
4101 H $\delta$	$22.77 \pm 1.68$	$32.22 \pm 3.63$	2.6	$20.10 \pm 0.85$	$26.18 \pm 1.44$	5.8
4340 H $\gamma$	$38.21 \pm 2.28$	$47.13 \pm 3.86$	4.3	$41.81 \pm 1.02$	$47.12 \pm 1.40$	13.9
4363 [O III]	$2.13 \pm 0.67$	$2.29 \pm 0.76$	0.2	$4.13 \pm 0.54$	$4.25 \pm 0.58$	1.2
4471 He I	...	...	...	$2.14 \pm 0.51$	$2.17 \pm 0.53$	0.6
4861 H $\beta$	$100.00 \pm 3.68$	$100.00 \pm 4.27$	13.5	$100.00 \pm 1.87$	$100.00 \pm 2.02$	40.4
4959 [O III]	$35.14 \pm 2.36$	$32.93 \pm 2.32$	4.2	$77.75 \pm 1.52$	$74.51 \pm 1.51$	29.5
5007 [O III]	$101.15 \pm 3.77$	$93.83 \pm 3.67$	12.0	$234.50 \pm 3.91$	$223.58 \pm 3.86$	89.0
5015 He I	...	...	...	$1.75 \pm 0.03$	$1.66 \pm 0.03$	0.7
$C(H\beta)$		0.405			0.205	
$F(H\beta)^b$		0.05			0.34	
EW(abs) Å		0.60			1.30	
GALAXY						
	J0946+5452			J0956+2849 No.1		
3727 [O II]	$178.39 \pm 5.59$	$208.41 \pm 6.99$	29.9	$30.46 \pm 0.81$	$39.18 \pm 1.08$	41.5
3750 H12	...	...	...	$2.29 \pm 0.34$	$4.77 \pm 0.90$	3.2
3771 H11	...	...	...	$2.37 \pm 0.35$	$4.68 \pm 0.85$	3.6
3798 H10	...	...	...	$3.18 \pm 0.36$	$5.73 \pm 0.80$	4.7
3835 H9	...	...	...	$5.04 \pm 0.36$	$8.09 \pm 0.75$	7.0
3868 [Ne III]	$27.44 \pm 2.24$	$31.29 \pm 2.62$	3.3	$10.28 \pm 0.44$	$12.74 \pm 0.56$	13.6
3889 He I + H8	$10.65 \pm 1.88$	$14.74 \pm 3.21$	1.8	$14.35 \pm 0.45$	$19.44 \pm 0.76$	20.3
3968 [Ne III] + H7	$11.55 \pm 1.44$	$15.63 \pm 2.70$	1.9	$15.54 \pm 0.66$	$20.56 \pm 1.00$	21.3
4101 H $\delta$	$19.65 \pm 1.75$	$24.11 \pm 2.78$	3.4	$20.29 \pm 0.50$	$25.39 \pm 0.75$	28.9
4340 H $\gamma$	$42.38 \pm 1.98$	$47.19 \pm 2.75$	7.5	$41.58 \pm 0.79$	$47.53 \pm 1.00$	60.5
4363 [O III]	$7.72 \pm 1.63$	$8.14 \pm 1.75$	1.0	$5.42 \pm 0.30$	$5.97 \pm 0.34$	8.2
4471 He I	...	...	...	$3.03 \pm 0.28$	$3.25 \pm 0.31$	4.8
4686 He II	...	...	...	$2.10 \pm 0.24$	$2.15 \pm 0.25$	3.3
4861 H $\beta$	$100.00 \pm 3.03$	$100.00 \pm 3.32$	21.9	$100.00 \pm 1.65$	$100.00 \pm 1.70$	187.9
4959 [O III]	$122.28 \pm 3.56$	$118.55 \pm 3.53$	20.2	$62.78 \pm 1.08$	$60.92 \pm 1.06$	109.7
5007 [O III]	$371.77 \pm 9.26$	$358.18 \pm 9.13$	63.1	$189.44 \pm 3.02$	$182.12 \pm 2.95$	326.5
$C(H\beta)$		0.245			0.370	
$F(H\beta)^b$		0.09			0.34	
EW(abs) Å		0.40			2.00	

Table 3—Continued

Ion	$F(\lambda)/F(H\beta)$	$I(\lambda)/I(H\beta)$	EW <sup>a</sup>	$F(\lambda)/F(H\beta)$	$I(\lambda)/I(H\beta)$	EW <sup>a</sup>
GALAXY						
	J0956+2849 No.2			J0956+2849 No.6		
3727 [O II]	54.36 ± 2.11	68.83 ± 2.76	71.9	125.24 ± 5.57	138.77 ± 6.69	44.6
3771 H11	3.49 ± 0.99	6.51 ± 2.17	7.2	...	...	...
3798 H10	4.97 ± 0.89	8.74 ± 2.03	8.6	...	...	...
3835 H9	6.75 ± 1.21	10.67 ± 2.23	12.6	...	...	...
3868 [Ne III]	8.45 ± 1.15	10.34 ± 1.43	14.3	8.62 ± 2.80	9.36 ± 3.19	2.6
3889 He I + H8	14.92 ± 1.90	20.15 ± 2.77	32.4	9.36 ± 1.90	15.19 ± 4.22	4.0
3968 [Ne III] + H7	15.61 ± 1.01	21.38 ± 1.89	24.2	6.88 ± 1.90	13.68 ± 5.44	2.3
4101 Hδ	20.06 ± 1.03	25.75 ± 1.77	32.7	21.54 ± 2.53	27.84 ± 4.14	8.7
4340 Hγ	41.50 ± 1.25	47.48 ± 1.69	85.1	41.51 ± 2.43	47.62 ± 3.74	15.9
4363 [O III]	4.04 ± 0.72	4.41 ± 0.80	9.0	5.56 ± 1.65	5.66 ± 1.76	1.7
4471 He I	3.30 ± 0.59	3.52 ± 0.65	7.6	5.37 ± 1.89	5.39 ± 1.99	1.9
4686 He II	6.19 ± 0.76	6.32 ± 0.79	16.4	...	...	...
4861 Hβ	100.00 ± 2.28	100.00 ± 2.38	294.2	100.00 ± 3.60	100.00 ± 4.18	45.8
4959 [O III]	44.81 ± 1.26	43.47 ± 1.24	145.0	48.67 ± 2.25	46.14 ± 2.23	20.0
5007 [O III]	138.05 ± 2.96	132.73 ± 2.90	540.1	153.05 ± 5.01	144.31 ± 4.95	61.7
$C(H\beta)$		0.350			0.205	
$F(H\beta)^b$		0.11			0.04	
EW(abs) Å		3.55			2.00	
GALAXY						
	J2238+1400 No.1			J2238+1400 No.2		
3188 He I	1.51 ± 0.22	2.04 ± 0.30	2.9	...	...	...
3679 H21	0.43 ± 0.07	0.52 ± 0.09	0.9	...	...	...
3683 H20	0.55 ± 0.10	0.67 ± 0.12	1.2	0.86 ± 0.18	1.23 ± 0.26	1.3
3687 H19	0.68 ± 0.10	0.83 ± 0.13	1.5	0.65 ± 0.13	0.94 ± 0.19	1.0
3692 H18	1.05 ± 0.11	1.28 ± 0.13	2.4	0.72 ± 0.13	1.03 ± 0.18	1.1
3697 H17	1.05 ± 0.11	1.27 ± 0.13	2.4	0.72 ± 0.13	1.03 ± 0.18	1.1
3704 H16	1.53 ± 0.11	1.86 ± 0.14	3.5	1.35 ± 0.17	1.93 ± 0.24	2.0
3712 H15	1.40 ± 0.10	2.03 ± 0.20	3.2	1.28 ± 0.22	1.83 ± 0.38	2.0
3722 H14	1.86 ± 0.09	2.25 ± 0.11	4.3	1.18 ± 0.09	1.67 ± 0.13	1.9
3727 [O II]	25.39 ± 0.41	30.68 ± 0.52	59.0	40.33 ± 0.69	57.08 ± 1.03	63.1
3750 H12	2.59 ± 0.12	3.45 ± 0.21	6.0	2.35 ± 0.18	3.29 ± 0.34	3.6
3771 H11	3.18 ± 0.12	4.15 ± 0.21	7.3	2.38 ± 0.17	3.31 ± 0.32	3.6
3798 H10	4.50 ± 0.14	5.70 ± 0.23	10.3	3.81 ± 0.18	5.26 ± 0.33	5.9
3820 He I	1.07 ± 0.10	1.27 ± 0.12	2.5	1.07 ± 0.14	1.46 ± 0.20	1.6
3835 H9	5.96 ± 0.15	7.40 ± 0.23	13.5	4.87 ± 0.20	6.64 ± 0.34	7.5
3868 [Ne III]	35.74 ± 0.55	42.05 ± 0.68	80.5	30.17 ± 0.54	40.67 ± 0.75	45.3
3889 He I + H8	14.41 ± 0.25	17.23 ± 0.34	32.5	14.26 ± 0.32	19.09 ± 0.49	21.0
3968 [Ne III] + H7	25.23 ± 0.40	29.46 ± 0.50	58.6	20.78 ± 0.40	27.10 ± 0.57	30.9
4026 He I	1.54 ± 0.09	1.75 ± 0.11	3.5	1.57 ± 0.17	2.01 ± 0.22	2.4
4101 Hδ	23.15 ± 0.36	26.40 ± 0.44	58.1	21.34 ± 0.40	26.65 ± 0.54	34.6
4143 He I	0.35 ± 0.05	0.39 ± 0.06	0.8	...	...	...
4227 [Fe V]	0.63 ± 0.06	0.70 ± 0.07	1.6	...	...	...
4340 Hγ	43.61 ± 0.65	47.48 ± 0.73	112.8	40.61 ± 0.66	47.09 ± 0.80	65.6
4363 [O III]	16.72 ± 0.27	18.04 ± 0.30	43.2	12.27 ± 0.26	14.14 ± 0.31	19.8

Table 3—Continued

Ion	$F(\lambda)/F(H\beta)$	$I(\lambda)/I(H\beta)$	EW <sup>a</sup>	$F(\lambda)/F(H\beta)$	$I(\lambda)/I(H\beta)$	EW <sup>a</sup>
4387 He I	$0.42 \pm 0.06$	$0.46 \pm 0.07$	1.1	...	...	...
4471 He I	$3.63 \pm 0.10$	$3.85 \pm 0.10$	9.9	$3.61 \pm 0.17$	$4.02 \pm 0.19$	6.2
4658 [Fe III]	$0.33 \pm 0.05$	$0.34 \pm 0.05$	0.9	...	...	...
4686 He II	$1.02 \pm 0.08$	$1.05 \pm 0.08$	3.1	$1.06 \pm 0.13$	$1.12 \pm 0.13$	2.0
4711 [Ar IV] + He I	$3.50 \pm 0.10$	$3.57 \pm 0.10$	10.5	$2.03 \pm 0.13$	$2.12 \pm 0.14$	3.7
4740 [Ar IV]	$2.33 \pm 0.08$	$2.37 \pm 0.08$	7.0	$1.37 \pm 0.13$	$1.42 \pm 0.14$	2.7
4861 H $\beta$	$100.00 \pm 1.46$	$100.00 \pm 1.47$	303.9	$100.00 \pm 1.52$	$100.00 \pm 1.54$	189.4
4921 He I	$0.91 \pm 0.07$	$0.90 \pm 0.07$	2.8	$0.91 \pm 0.10$	$0.89 \pm 0.10$	1.8
4959 [O III]	$168.98 \pm 2.45$	$166.24 \pm 2.43$	510.5	$164.67 \pm 2.47$	$160.48 \pm 2.43$	320.0
4988 [Fe III]	$0.58 \pm 0.07$	$0.57 \pm 0.07$	1.7	...	...	...
5007 [O III]	$506.95 \pm 7.31$	$495.33 \pm 7.19$	1531.5	$494.02 \pm 7.33$	$475.50 \pm 7.11$	960.0
$C(H\beta)$		0.270			0.490	
$F(H\beta)^b$		2.52			0.99	
EW(abs) Å		0.65			0.00	

<sup>a</sup>in Å.

<sup>b</sup>in units  $10^{-14}$  erg s<sup>-1</sup> cm<sup>-2</sup>.

Table 4. IONIC AND TOTAL HEAVY ELEMENT ABUNDANCES

PROPERTY	Value	Value	Value	Value
GALAXY				
	J0113+0052 No.1	J0113+0052 No.2	J0113+0052 No.4	J0204-1009 No.1
$T_e(\text{O III})$ (K)	$19963 \pm 1290$	$18766 \pm 1011$	$18330 \pm 1009$	$18417 \pm 1032$
$T_e(\text{O II})$ (K)	$16278 \pm 932$	$16014 \pm 1255$	$15883 \pm 1244$	$15911 \pm 1274$
$\text{O}^+/\text{H}^+$ ( $\times 10^4$ )	$0.056 \pm 0.008$	$0.139 \pm 0.027$	$0.082 \pm 0.016$	$0.125 \pm 0.026$
$\text{O}^{++}/\text{H}^+$ ( $\times 10^4$ )	$0.118 \pm 0.017$	$0.081 \pm 0.010$	$0.140 \pm 0.018$	$0.107 \pm 0.015$
$\text{O}/\text{H}$ ( $\times 10^4$ )	$0.174 \pm 0.019$	$0.220 \pm 0.029$	$0.222 \pm 0.025$	$0.232 \pm 0.030$
$12 + \log(\text{O}/\text{H})$	$7.240 \pm 0.048$	$7.343 \pm 0.057$	$7.347 \pm 0.048$	$7.365 \pm 0.057$
$\text{Ne}^{++}/\text{H}^+$ ( $\times 10^5$ )	$0.235 \pm 0.038$	...	$0.211 \pm 0.030$	$0.331 \pm 0.081$
ICF	1.116	...	1.139	1.239
$\log(\text{Ne}/\text{O})$	$-0.821 \pm 0.104$	...	$-0.966 \pm 0.088$	$-0.753 \pm 0.188$
GALAXY				
	J0204-1009 No.2	J0254+0035	J0301-0052	J0313+0010
$T_e(\text{O III})$ (K)	$16534 \pm 665$	$19285 \pm 1013$	$17257 \pm 1125$	$17839 \pm 1028$
$T_e(\text{O II})$ (K)	$15148 \pm 553$	$16146 \pm 1269$	$15482 \pm 913$	$15714 \pm 1257$
$\text{O}^+/\text{H}^+$ ( $\times 10^4$ )	$0.123 \pm 0.012$	$0.111 \pm 0.022$	$0.049 \pm 0.008$	$0.160 \pm 0.034$
$\text{O}^{++}/\text{H}^+$ ( $\times 10^4$ )	$0.239 \pm 0.024$	$0.079 \pm 0.010$	$0.285 \pm 0.045$	$0.114 \pm 0.017$
$\text{O}/\text{H}$ ( $\times 10^4$ )	$0.361 \pm 0.027$	$0.190 \pm 0.024$	$0.335 \pm 0.046$	$0.274 \pm 0.037$
$12 + \log(\text{O}/\text{H})$	$7.558 \pm 0.032$	$7.279 \pm 0.055$	$7.524 \pm 0.060$	$7.438 \pm 0.059$
$\text{Ne}^{++}/\text{H}^+$ ( $\times 10^5$ )	$0.476 \pm 0.050$	$0.132 \pm 0.033$	$0.537 \pm 0.093$	...
ICF	1.125	1.271	1.048	...
$\log(\text{Ne}/\text{O})$	$-0.829 \pm 0.070$	$-1.053 \pm 0.214$	$-0.774 \pm 0.103$	...
GALAXY				
	J0747+5111 No.1	J0747+5111 No.2	J0812+4836	J0859+3923
$T_e(\text{O III})$ (K)	$15816 \pm 832$	$15694 \pm 412$	$19634 \pm 1013$	$16799 \pm 1015$
$T_e(\text{O II})$ (K)	$14765 \pm 708$	$14695 \pm 352$	$16220 \pm 1276$	$15276 \pm 1221$
$\text{O}^+/\text{H}^+$ ( $\times 10^4$ )	$0.229 \pm 0.030$	$0.155 \pm 0.010$	$0.140 \pm 0.027$	$0.237 \pm 0.049$
$\text{O}^{++}/\text{H}^+$ ( $\times 10^4$ )	$0.345 \pm 0.046$	$0.375 \pm 0.025$	$0.049 \pm 0.006$	$0.134 \pm 0.020$
$\text{O}^{+++}/\text{H}^+$ ( $\times 10^6$ )	...	$0.562 \pm 0.146$	...	...
$\text{O}/\text{H}$ ( $\times 10^4$ )	$0.574 \pm 0.055$	$0.536 \pm 0.027$	$0.189 \pm 0.028$	$0.372 \pm 0.054$
$12 + \log(\text{O}/\text{H})$	$7.759 \pm 0.041$	$7.729 \pm 0.022$	$7.276 \pm 0.064$	$7.570 \pm 0.063$
$\text{Ne}^{++}/\text{H}^+$ ( $\times 10^5$ )	$0.800 \pm 0.114$	$0.778 \pm 0.057$	$0.086 \pm 0.025$	$0.324 \pm 0.081$
ICF	1.155	1.106	1.390	1.309
$\log(\text{Ne}/\text{O})$	$-0.793 \pm 0.098$	$-0.795 \pm 0.047$	$-1.196 \pm 0.354$	$-0.943 \pm 0.238$
GALAXY				
	J0911+3135	J0940+2935	J0946+5452	J0956+2849 No.1
$T_e(\text{O III})$ (K)	$16641 \pm 2792$	$14889 \pm 923$	$16192 \pm 1722$	$19676 \pm 685$
$T_e(\text{O II})$ (K)	$15200 \pm 2315$	$14196 \pm 806$	$14971 \pm 1449$	$16228 \pm 502$
$\text{O}^+/\text{H}^+$ ( $\times 10^4$ )	$0.243 \pm 0.096$	$0.200 \pm 0.032$	$0.190 \pm 0.048$	$0.028 \pm 0.002$

Table 4—Continued

PROPERTY	Value	Value	Value	Value
$O^{++}/H^+ (\times 10^4)$	$0.081 \pm 0.034$	$0.250 \pm 0.041$	$0.326 \pm 0.087$	$0.108 \pm 0.009$
$O^{+++}/H^+ (\times 10^6)$	...	...	...	$0.352 \pm 0.047$
$O/H (\times 10^4)$	$0.325 \pm 0.101$	$0.451 \pm 0.051$	$0.516 \pm 0.099$	$0.139 \pm 0.009$
$12 + \log(O/H)$	$7.511 \pm 0.136$	$7.654 \pm 0.049$	$7.713 \pm 0.083$	$7.144 \pm 0.028$
$Ne^{++}/H^+ (\times 10^5)$	$0.248 \pm 0.132$	$0.430 \pm 0.077$	$0.674 \pm 0.187$	$0.168 \pm 0.014$
ICF	1.398	1.180	1.139	1.075
$\log(Ne/O)$	$-0.972 \pm 0.674$	$-0.948 \pm 0.128$	$-0.827 \pm 0.187$	$-0.888 \pm 0.053$
GALAXY				
	J0956+2849 No.2	J0956+2849 No.6	J2238+1400 No.1	J2238+1400 No.2
$T_e(O \text{ III})$ (K)	$19913 \pm 2184$	$22170 \pm 4668$	$20975 \pm 268$	$18580 \pm 260$
$T_e(O \text{ II})$ (K)	$16270 \pm 1583$	$16396 \pm 2938$	$16392 \pm 183$	$15961 \pm 201$
$O^+/H^+ (\times 10^4)$	$0.049 \pm 0.012$	$0.096 \pm 0.042$	$0.021 \pm 0.001$	$0.043 \pm 0.002$
$O^{++}/H^+ (\times 10^4)$	$0.076 \pm 0.019$	$0.067 \pm 0.030$	$0.257 \pm 0.008$	$0.318 \pm 0.011$
$O^{+++}/H^+ (\times 10^6)$	$0.878 \pm 0.192$	...	$0.295 \pm 0.024$	$0.395 \pm 0.049$
$O/H (\times 10^4)$	$0.134 \pm 0.022$	$0.163 \pm 0.052$	$0.282 \pm 0.008$	$0.365 \pm 0.011$
$12 + \log(O/H)$	$7.127 \pm 0.072$	$7.212 \pm 0.137$	$7.450 \pm 0.012$	$7.562 \pm 0.013$
$Ne^{++}/H^+ (\times 10^5)$	$0.132 \pm 0.036$	$0.094 \pm 0.050$	$0.478 \pm 0.015$	$0.614 \pm 0.022$
ICF	1.173	1.275	1.030	1.042
$\log(Ne/O)$	$-0.936 \pm 0.189$	$-1.132 \pm 0.464$	$-0.758 \pm 0.019$	$-0.757 \pm 0.022$
$Fe^{++}/H^+(\times 10^6)(4658)$	...	...	$0.052 \pm 0.008$	...
$Fe^{++}/H^+(\times 10^6)(4988)$	...	...	$0.088 \pm 0.011$	...
ICF	...	...	18.255	...
$\log(Fe/O)$ (4658)	...	...	$-1.475 \pm 0.068$	...
$\log(Fe/O)$ (4988)	...	...	$-1.244 \pm 0.055$	...

Table 5. Oxygen abundances derived by different methods

SDSS Name	$12+\log\text{O}/\text{H}^{\text{a}}$	$12+\log\text{O}/\text{H}^{\text{b}}$	$12+\log\text{O}/\text{H}^{\text{c}}$	$12+\log\text{O}/\text{H}^{\text{d}}$	$12+\log\text{O}/\text{H}^{\text{e}}$
SDSSJ0113+0052 No.1	$7.24\pm 0.05$	7.35	7.16	7.25	$7.29\pm 0.04$
SDSSJ0113+0052 No.2	...	7.48	7.16	7.25	$7.34\pm 0.06$
SDSSJ0113+0052 No.4	...	7.44	7.20	7.30	$7.35\pm 0.05$
SDSSJ0204–1009 No.1	...	7.52	7.19	7.29	$7.37\pm 0.06$
SDSSJ0204–1009 No.2	$7.56\pm 0.03$	7.60	7.38	7.47	$7.55\pm 0.05$
SDSSJ0254+0035	...	7.45	7.11	7.20	$7.28\pm 0.05$
SDSSJ0301–0052	$7.52\pm 0.06$	7.44	7.44	7.52	$7.59\pm 0.06$
SDSSJ0313+0010	...	7.58	7.25	7.35	$7.44\pm 0.06$
SDSSJ0747+5111 No.1	$7.75\pm 0.04$	7.96	7.70	7.68	$7.84\pm 0.06$
SDSSJ0747+5111 No.2	$7.73\pm 0.02$	7.78	7.62	7.64	$7.78\pm 0.06$
SDSSJ0812+4836	...	7.35	7.08	7.16	$7.28\pm 0.06$
SDSSJ0859+3923	...	7.69	7.36	7.45	$7.57\pm 0.06$
SDSSJ0911+3135	$7.51\pm 0.14$	7.46	7.24	7.34	$7.46\pm 0.05$
SDSSJ0940+2935	$7.65\pm 0.05$	7.65	7.35	7.45	$7.53\pm 0.04$
SDSSJ0946+5452	$7.71\pm 0.08$	7.88	7.64	7.66	$7.80\pm 0.06$
SDSSJ0956+2849 No.1	$7.14\pm 0.03$	7.16	7.04	7.12	$7.13\pm 0.04$
SDSSJ0956+2849 No.2	$7.13\pm 0.07$	7.26	7.00	7.03	$7.10\pm 0.03$
SDSSJ0956+2849 No.6	$7.21\pm 0.14$	7.45	7.12	7.21	$7.28\pm 0.04$
SDSSJ2238+1400 No.1	$7.45\pm 0.01$	7.51	7.66	7.66	$7.78\pm 0.07$
SDSSJ2238+1400 No.2	$7.56\pm 0.01$	7.57	7.66	7.66	$7.79\pm 0.07$
$\Delta(12+\log\text{O}/\text{H})^{\text{f}}$	...	0.10	0.13	0.07	0.06

<sup>a</sup> $T_e(\text{O III})$  is derived from the  $[\text{O III}] \lambda 4363/(\lambda 4959+\lambda 5007)$  ratio (direct method).

<sup>b</sup> $12 + \log\text{O}/\text{H}$  is derived from Eq. 2 (Pilyugin & Thuan 2005) (empirical method).

<sup>c</sup> $12 + \log\text{O}/\text{H}$  is derived from Eq. 3 (Nagao et al. 2006) (empirical method).

<sup>d</sup> $12 + \log\text{O}/\text{H}$  is derived from Eq. 4 (Yin et al. 2007) (empirical method).

<sup>e</sup> $T_e(\text{O III})$  is derived from Eq. 1 (semi-empirical method).

<sup>f</sup>Average difference between the empirical abundances and those derived by the direct method, excluding the two H II regions in J2238+1400.

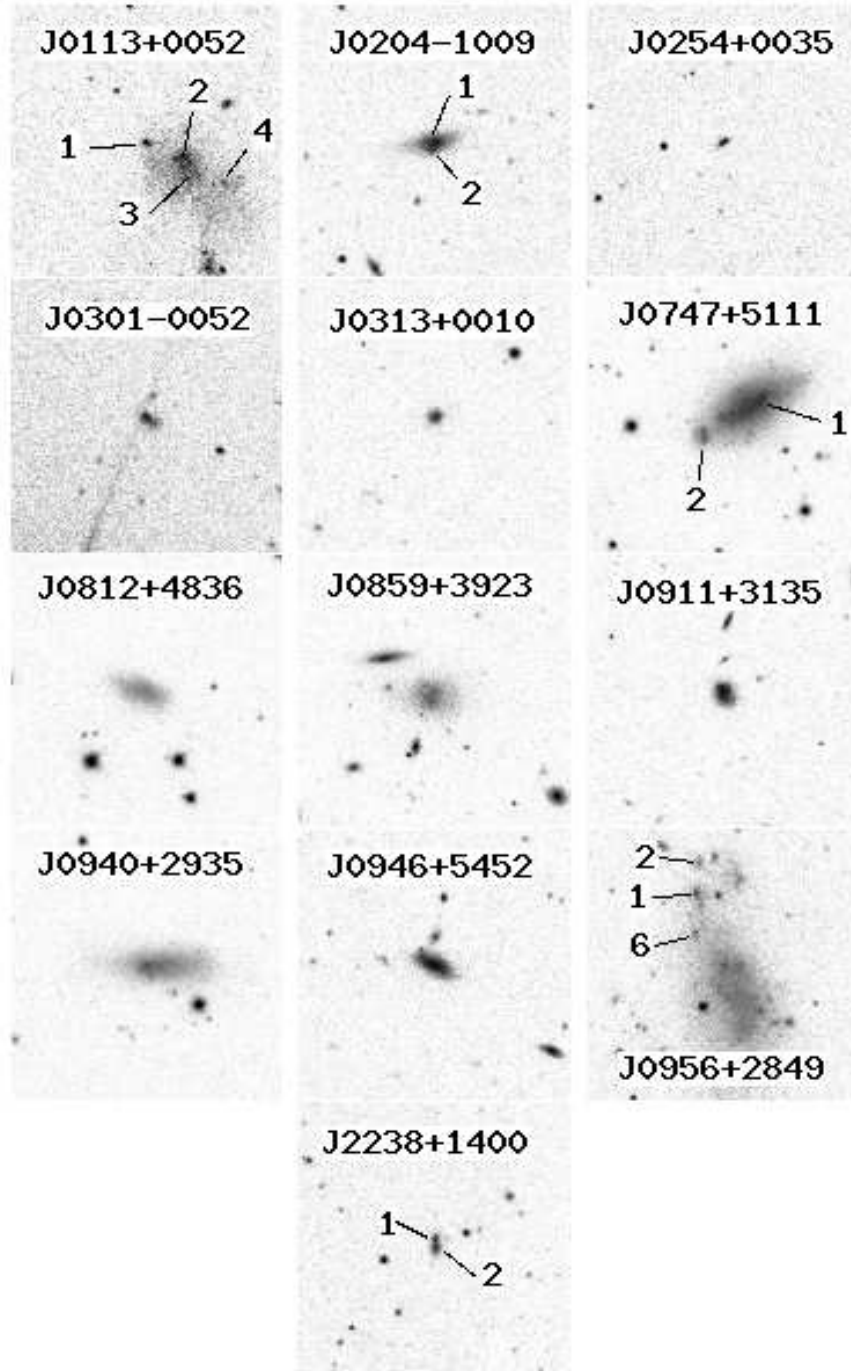


Fig. 1.— SDSS images of galaxies in MMT subsample.

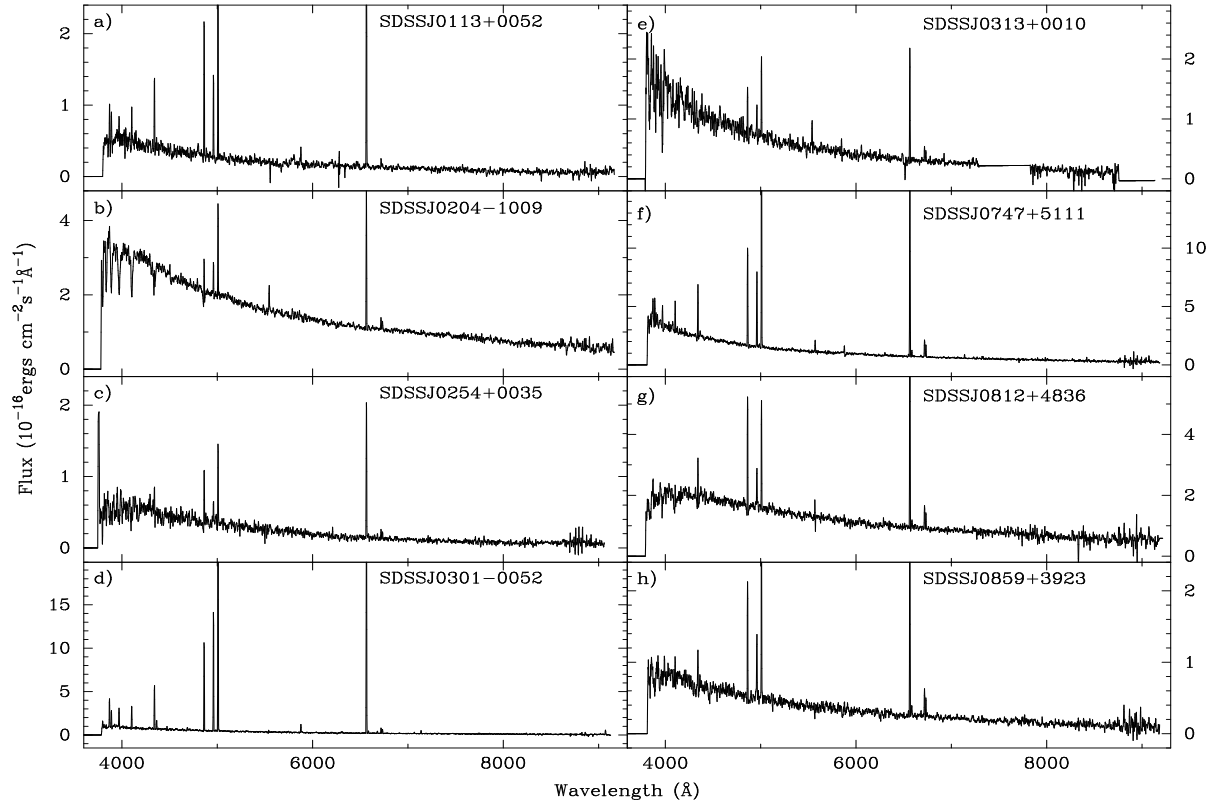


Fig. 2.— SDSS spectra of galaxies in MMT subsample.



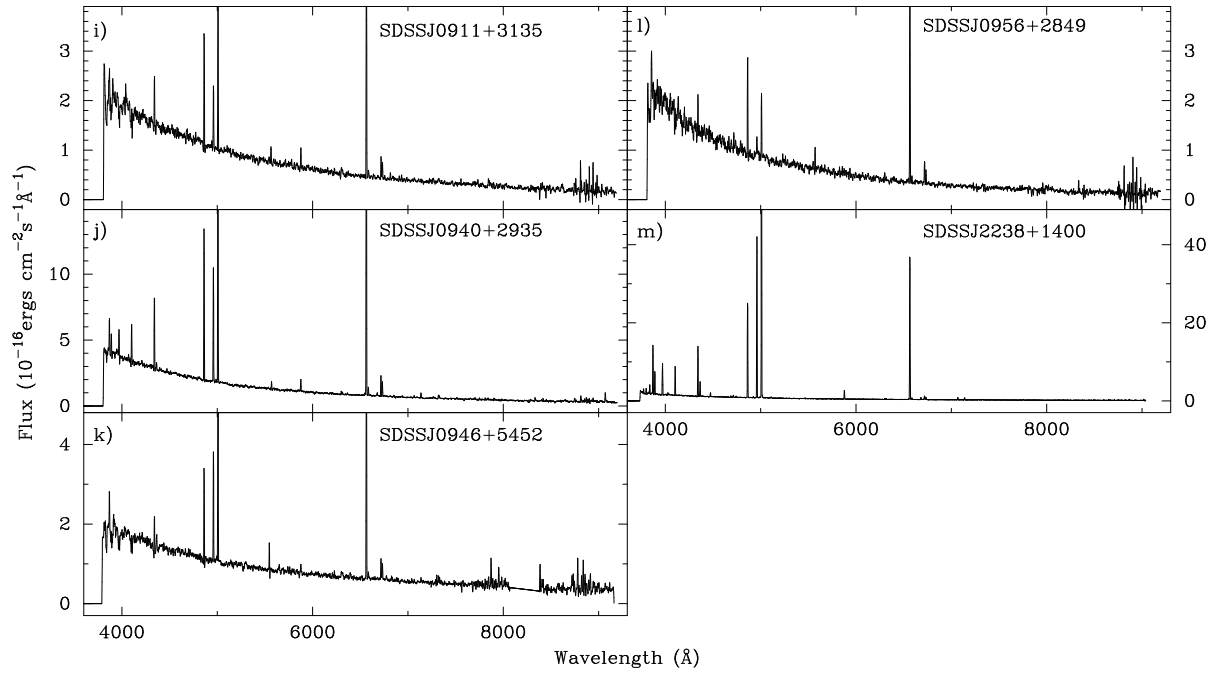


Fig. 2.— Continued.

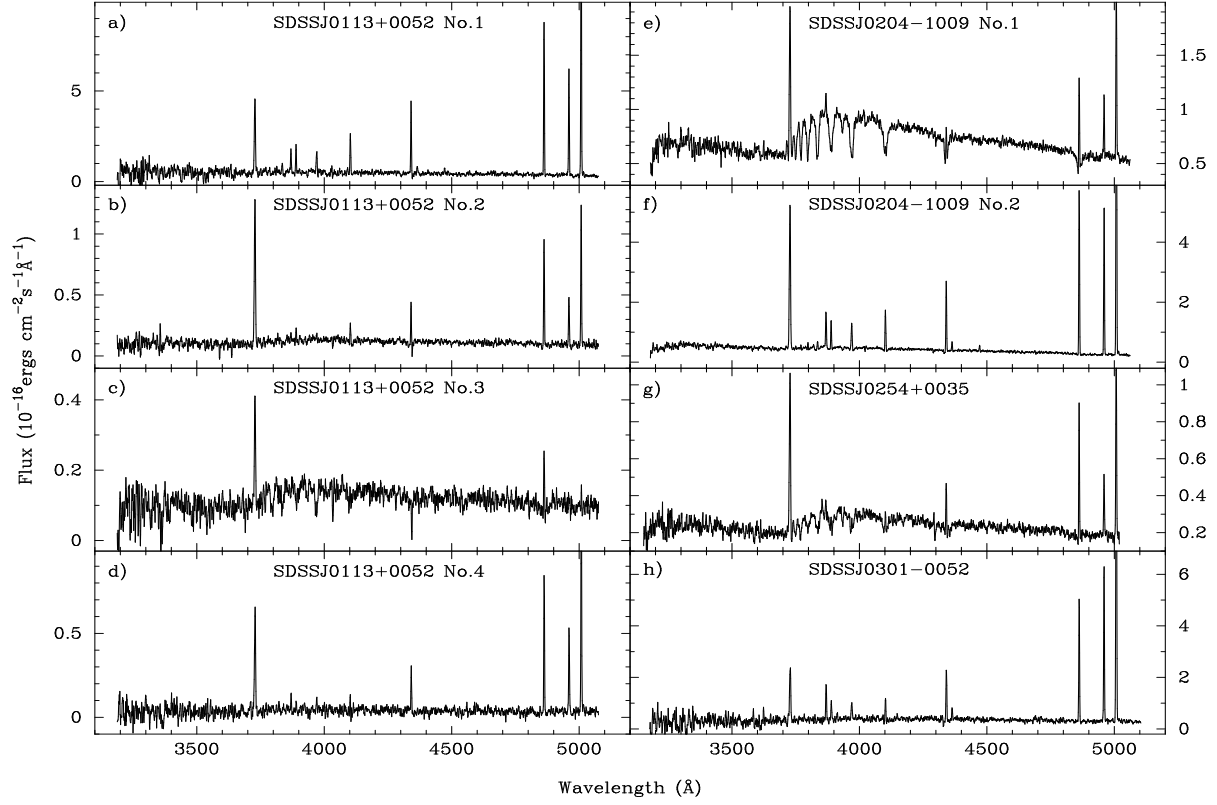


Fig. 3.— MMT spectra of extremely low-metallicity SDSS galaxies. The inset in panel t shows a blow-up of the blue part of the spectrum.

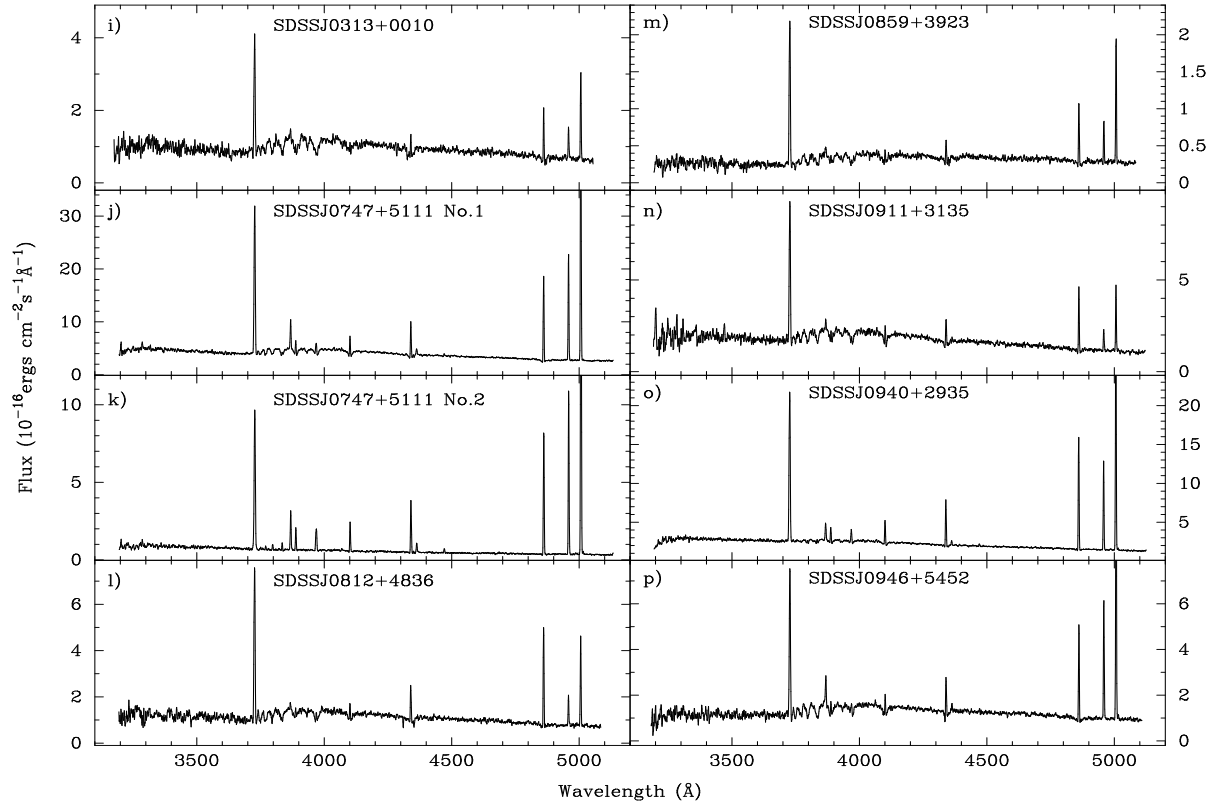


Fig. 3.— Continued.

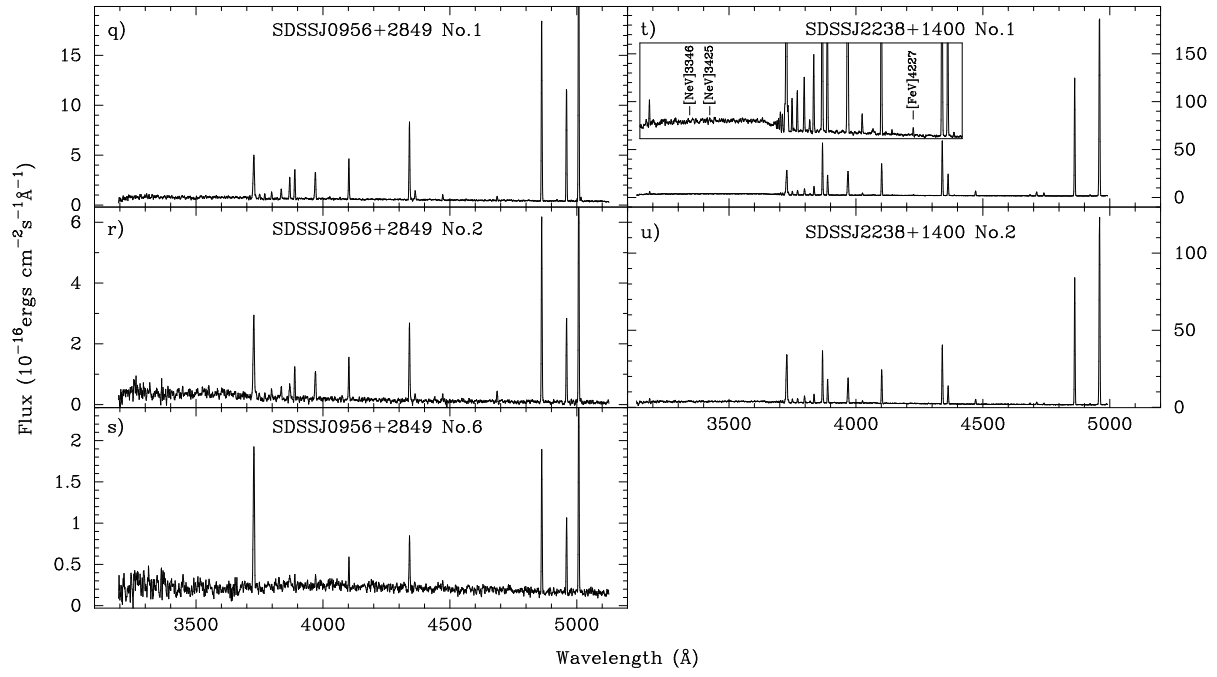


Fig. 3.— Continued.